THE JOURNAL OF PHYSICAL CHEMISTRY LETTERS
A JOURNAL OF THE AMERICAN CHEMICAL SOCIETY

pubs.acs.org/JPCL
Letter

Toward Generalized Solution-State ^{1}H DNP NMR via Particle-Mediated Cross-Relaxation

Sungsool Wi,* Angeliki Giannouli, Korin Butbul, Jenica Lumata, Thierry Dubroca, Faith Scott, Zachary Dowdell, Robert W. Schurko, Hans Van Tol, and Lucio Frydman*

Cite This: J. Phys. Chem. Lett. 2025, 16, 6627−6636
Read Online

ACCESS | Metrics & More | Article Recommendations | Supporting Information

ABSTRACT: This study discusses a potential route for enhancing ^{1}H NMR signals in the liquid phase at high magnetic fields for samples on the 100 μL volume scale using dynamic nuclear polarization (DNP). The approach involves dispersing an inert powder that is both rich in protons and capable of undergoing DNP with good efficiency at noncryogenic temperatures, and letting the solid ^{1}H polarization thus enhanced pass from the dispersed particles onto the surrounding liquid via spontaneous cross relaxation effects. To this end, BDPA-doped polystyrene (PS) particles in the μm range were suspended in 30 μL of heptane, loaded into 3.2 mm sapphire rotors, and spun at ≈500 Hz for homogeneity purposes in a 14.1 T magnet. Irradiation with ≈13 W at 395 GHz while maintaining temperature in the 185−220 K range thus enhanced the PS proton polarization ≈12-fold within ≈2 s; after ca. 6 s of irradiation, this resulted in ca. 3-fold enhancements of the heptane proton resonances, while preserving their ≤2 Hz line widths. The conditions over which such particle-mediated transfer occurs were explored over a range of sample composition, deuteration and molecular weight; best results were obtained when polarizing a ball-milled powder made of deuterated-PS/PS/BDPA = 86.4/9.6/4.0 suspended on perdeuterated heptane-d_{16}. While the solution-state enhancements provided by this approach are still relatively modest, its generality could open new avenues in DNP-enhanced ^{1}H NMR that do not sacrifice on the volumes, on the high-resolution conditions, or on the multiscan averaging that is customary in contemporary applications.

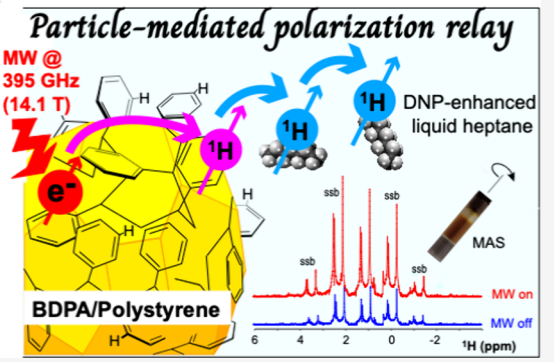

Although NMR is a powerful tool for characterizing molecular structure and dynamics,[1−4] it suffers from poor sensitivity. This reflects the low polarization levels reached by nuclear spins at ambient temperature, even when placed in high magnetic fields.[1] By transferring order from more highly polarized, comixed electrons, dynamic nuclear polarization (DNP) can dramatically boost NMR's sensitivity.[5−7] The past decade has seen much of this enhancement potential enabled for solid-state NMR, in experiments combining Gyrotron-based high-power microwave (μwave) irradiation, with the cryogenic conditions needed for enabling a saturation of the electronic spin.[8−11] Early successes at low fields (B_0 < 1 T)[12−18] also bode well for the potential of solution-state DNP NMR; this, however, has yet to reach maturity due to the nearly negligible spectral densities needed for a generic electron → nuclear cross-relaxation-driven transfer, at the higher B_0 fields of interest in analytical NMR. Foremost among the alternatives that have been stimulated by liquid-state NMR's needs stands dissolution DNP, which bypasses liquid-imposed limitations by performing the polarizing process at cryogenic (≈1 K) temperatures and then suddenly melting and flushing the sample pellet as a solution for room-temperature high field observations.[16] This has launched a revolution in metabolic imaging,[19−21] yet the relatively high dilution that this method requires, its limitation to sites with slow-relaxation and nuclides with low-γ values, and its "single-shot" nature constrain its analytical uses.[22−25] Further efforts have included low/high field sample shuttling experiments,[14,26−28] rapid sample melting followed by subsequent refreezing and repolarization,[29−32] and proposals based on biradicals.[33,34] *In situ* applications based on the Overhauser-Effect DNP (OE DNP) effect have also been demonstrated at high fields and on relatively large samples, based on scalar electron/nuclear interactions.[27,35−38] At high magnetic fields, however, OE DNP enhancements are critically dependent on the presence of substantial Fermi contacts, and hence limited to certain electronic environments; in particular, scalar-based OE DNP is of negligible use in the most common of all analytical NMR experiments: 1D ^{1}H NMR.[38−41] Closer to the spirit driving this study, OE DNP demonstrations

Received: May 9, 2025
Revised: June 4, 2025
Accepted: June 6, 2025
Published: June 20, 2025

carried out entirely in the liquid state at high magnetic fields based on high-power, high-efficiency microwave technologies have been reported,[42−45] based on ubiquitous electron−proton dipolar effects.[46−48] While these approaches could provide a general means to enhance protons in any molecule, these high-frequency, high-intensity microwave field experiments are compatible only with small, nanoliter-sized sample volumes. Water-oriented proposals that are somewhat related to the present study have been recently demonstrated, whereby hyperpolarization achieved on optically excited nanocrystals is relayed to the H_2O protons, via low field microwave-based manipulations, followed by solid → solution cross-relaxation among protons.[49,50]

Inspired by these developments, the present study explores a complementary, potentially generic approach to enhance solution state ^{1}H NMR at high fields, while targeting organic samples in the tens of μL. Dielectric losses limit such large-sample, high-field approaches to minimally absorbing solvents; while this leaves high-field water studies outside its realm, it should still be possible to target a considerable part of the organic/pharmaceutical NMR world with this kind of experiments. Making an organic-oriented DNP approach general would also demand a reliance on dipolar DNP effects, but as mentioned, these have negligible ^{1}H efficiencies in high-field NMR. To overcome this pitfall, we propose an experiment that targets a solid powder that will still undergo an efficient, solid-like DNP enhancement, even while dispersed in an organic solvent. Further, we propose choosing these particles to be sufficiently small in size and sufficiently rich in protons, to enable their DNP-enhanced ^{1}H polarizations to spontaneously spread into the liquid phase via ^{1}H−^{1}H cross relaxation; this in turn will have to be aided by solvent diffusivity in-and-out of the polarizing particles' surfaces, and by relatively long relaxation times T_1 so that a large number of molecules in the solution's bulk can come into contact with the polarizing particles.[50] The emerging Particle-Mediated DNP (PM-DNP, Scheme 1) proposal that is hereby discussed

Scheme 1. Representation of the PM-DNP Approach Adopted in This Study, to Polarize a Liquid with the Aid of Dispersed Particles Undergoing Efficient Microwave-Driven OE DNP in the Solid State

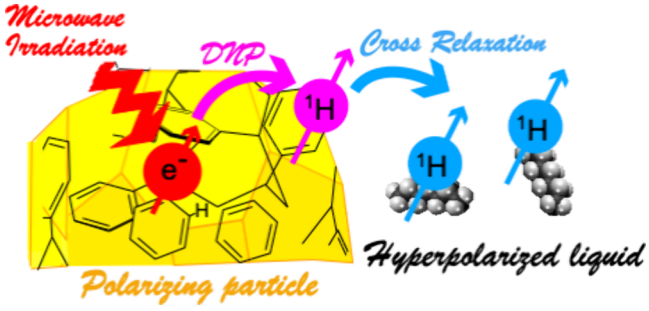

therefore not only has points in common with the aforementioned work by Prisner, Yanai et al.[45,49,50] but also has clear differences. In particular, the polarizing particles in PM-DNP will simultaneously have to fulfill two seemingly irreconcilable tasks: undergo high-field electron → nuclear polarization as if they were a solid and be dispersed in a medium with which they can undergo efficient cross-relaxation as if they were in a liquid. A number of solute/solvent systems could be used to achieve these dual roles; in the present study, attention centered on polystyrene (PS) as prototypical example. PS is available on a large range of micro- and nanoparticulate sizes and is often used as DNP calibration sample thanks to its ability to undergo efficient Overhauser and/or Solid Effect (OE, SE) enhancements over a wide range of temperatures and of magnetic fields.[8,51−53] In particular, when doped with 1,3-bis(diphenylene)-2-phenylallyl (BDPA), it has been shown[53,54] that a certain degree of deuteration helps in enhancing the efficiency of PS's DNP enhancement, including at high temperatures. For the present study, mixtures of conventional and deuterated polystyrene (dPS, with all the eight hydrogens in the monomers replaced by ^{2}H) were thus assayed, until reaching a suitable combination; also, a variety of solvents on which to test the transfer of DNP-enhanced polarization to solutions was assayed. In the end heptane, a solvent with low dielectric losses that will not dissolve PS nor BDPA, was identified as a suitable medium to assess these proposals. Also, in this case, heptane deuteration was found beneficial, presumably because it lengthened the solvent's T_1 and thereby enabled the DNP-derived buildup to proceed further throughout the full sample volume.

Figure 1 illustrates representative solid-state characteristics of the BDPA-doped PS samples analyzed in this study, recorded at 230 K while undergoing magic angle spinning (MAS) at ≈6 kHz (see Experimental Section for further details). The ^{1}H DNP field sweep profiles arising from the powders reveal a strong OE DNP enhancement at a field of 14.107 T, corresponding to a ^{1}H resonance frequency of 600.65 MHz and an electron Larmor frequency of 395.417 GHz, the latter being dictated by our Gyrotron's fixed output frequency. Further sweeps of the magnetic field evidence a second, SE-enhanced DNP effect occurring at B_0 = 14.085 T—equivalent to an electron frequency shift from the main OE event by 599.72 MHz, corresponding in turn to a shift by the ^{1}H Larmor frequency. These plots were recorded for samples where the dPS had high (431 kDa) and low (2.2 kDa) average molecular weights (HM_W, LM_W), while keeping the weight ratio of the three components in the mixture—dPS/PS/BDPA—constant at 86.4/9.6/4.0. The HM_W sample exhibited a larger ^{1}H DNP enhancement (ε = 19.3 over thermal at the OE condition) than the LM_W sample counterpart (ε = 11.4 at the OE condition). Figure 1 panels b and c show the μwave on/off signal build-up curves for the ^{1}Hs in these samples, as measured at the optimal OE DNP (600.65 MHz ^{1}H Larmor) position. For the microwave-off case, both samples exhibit similar 1.4−1.5 s build-up times. When the microwave was turned on, the HM_W dPS sample showed a build-up time that was approximately twice as long as that of the LM_W one and a concomitantly higher enhancement level. These differences likely reflect the different environments felt by the BDPA dopant in the PS matrix, where chain mobility and thereby electronic relaxation properties will be influenced by molecular weight. Figure 1 panels d and e complement these solid NMR results with ^{1}H MAS and ^{1}H−^{13}C CPMAS NMR spectra recorded for the LM_W sample, showing a similar $\varepsilon \approx 11$ OE DNP enhancement for both spectra.

As our aim is to enhance ^{1}H solution-state NMR by transferring the amplified ^{1}H polarization arising in the DNP-enhanced dPS/PS particles, these were ball-milled into fine powders before dispersing them into a solution. This should help leverage the intermolecular ^{1}H−^{1}H cross relaxation between the surface ^{1}Hs of fine dPS/PS particles and the solvent. Hexane and heptane were tested as the latter, since

https://doi.org/10.1021/acs.jpclett.5c01398
J. Phys. Chem. Lett. 2025, 16, 6627−6636

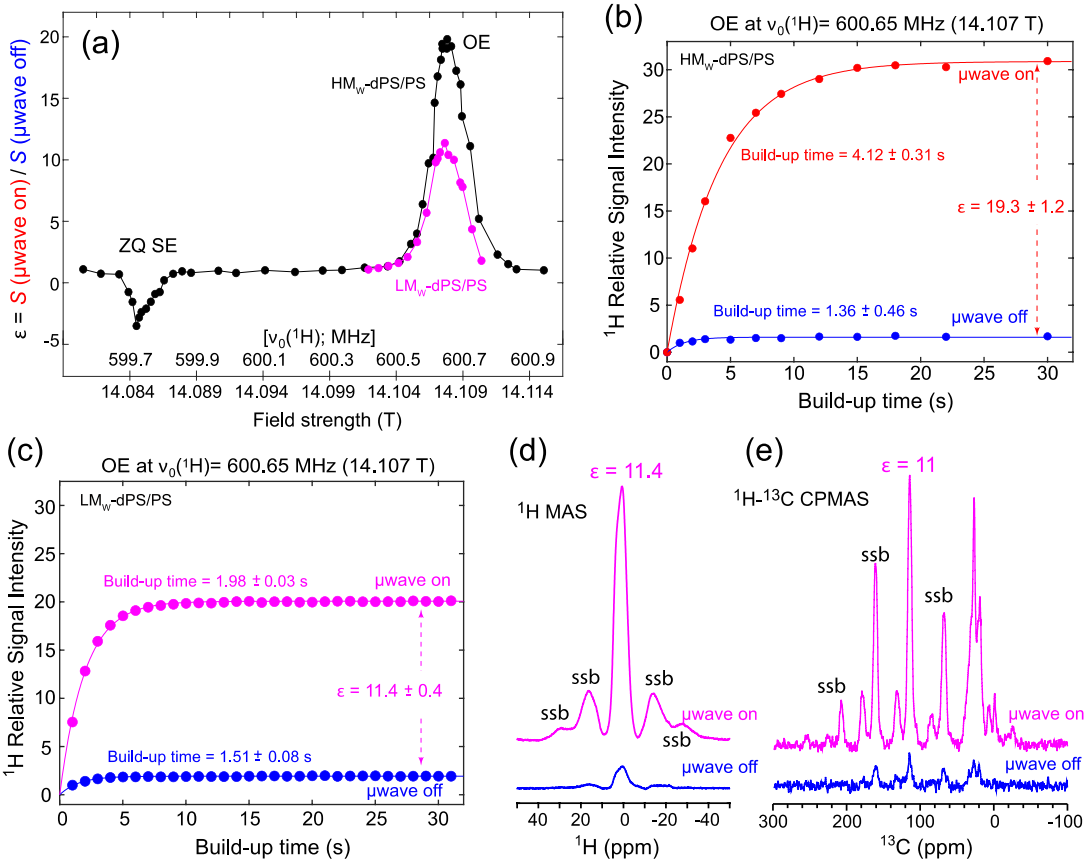

Figure 1. (a) DNP field sweep profiles of BDPA-doped dPS/PS solid samples containing high molecular weight (HM_W) (431 kDa; black) and low molecular weight (LM_W) (2.23 kDa; pink) dPS. Both samples comixed with nondeuterated PS (MW = 280 kDa) at a dPS/PS weight ratio of 90/10, with w/w 4% BDPA doped into the polymer matrix. Indicated are the positions of the Overhauser Effect (OE) and Zero-Quantum Solid Effect (ZQ SE) observed at the indicated field strengths, upon sweeping the magnetic field (and thereby the ^{1}H Larmor frequency, which changed as indicated) while keeping the electron irradiation frequency constant. (b, c) Microwave on/off build-up curves observed at the central OE position for the HM_W and LM_W dPS samples, respectively. (d, e) Corresponding ^{1}H MAS spectra and ^{13}C CPMAS NMR spectra arising for the LM_W dPS sample, in the presence and absence of μwave irradiation at the OE condition. Data in (a−c) arose from ^{1}H NMR spectra (e.g., d) recorded following a saturation recovery sequence, $[90° (^1H) - 1\ ms]_n - \tau_{buildup}$ (n = 50), with 13 W of μwave irradiation alternated between on and off states during the signal build-up time $\tau_{buildup}$. A 90° - τ_1 - 180° - τ_2 echo sequence was applied after $\tau_{buildup}$, with τ_1 = 250 μs and τ_2 = 0 μs; for ensuring thermal stability, experiments included a 60−80 s recycling delay. In (e), a 1 ms long CP block was included after $\tau_{buildup}$ to transfer ^{1}H magnetization to ^{13}C, with $\nu_1(^{13}C)$ = 50 kHz and $\nu_1(^1H)$ = 55 kHz (using a 70−110% ramp). Sixteen scans were coadded with SPINAL-64 ^{1}H decoupling (^{1}H rf ≈100 kHz).[55] Throughout all experiments, samples were spun at approximately 6 kHz, and the temperature was maintained at 230 K. ssb denotes spinning sidebands.

these do not dissolve BDPA or PS, and are minimal absorbers of microwaves. In the end, the focus was on heptane, as its higher boiling point (99 °C) allowed it to better withstand microwave heating. Addition trial-and-error tests (data not shown) led us to adopt fully perdeuterated heptane-d_{16} (99 atom % D) as preferred medium, as it led to the highest enhancements when focused on its residual ^{1}H nuclei.

With this as background, Figure 2a shows EPR spectra recorded on the microsized particles of BDPA-doped dPS/PS employing a LM_W sample. Two samples are here examined: a "wet precipitate" remaining after the PS particles are suspended in hexane or heptane and then settle in the bottom of an Eppendorf; and a more translucent "supernatant" containing particles that remain in suspension (see Supporting Information Section 1 for further description of these samples). These spectra were measured at 240 GHz, the closest that in EPR frequency could be accessed to the DNP NMR experiment, as well as at X-band (9.7 GHz). The high field EPR spectra recorded for the wet precipitate and for the supernatant present line shapes which are similar among themselves, as well as to the solid powder. By contrast, the X-band spectra of the supernatant, and to some extent also of the "wet precipitate" samples, display a fine structure that we attribute to a now-resolved e^--^{1}H hyperfine interaction. The supernatant line shape also indicates that the dispersed particles are tumbling fast enough to average out the anisotropic hyperfine interaction, whereas the slower tumbling of "wet" sample has a broadening reflecting incomplete motional averaging. EasySpin simulations[56] were performed to estimate rotational correlation times from these data (Supporting Information, Section 2): a radical correlation time of 2×10^{-7} s can account for both the X-band and 240 GHz supernatant sample spectra, while a slower correlation time ($\geq 3 \times 10^{-7}$ s) is required to fit the EPR spectrum of the wet precipitate. Assuming radicals that are fixed to the PS environs, these correlation time estimates predict particle sizes in the order of 1 μm. Dynamic light scattering experiments performed on similar samples (Supporting Information, Section 3) indicate larger particle diameters (≈4 μm); this probably reflects the respective biases of the EPR and DLS

https://doi.org/10.1021/acs.jpclett.5c01398
J. Phys. Chem. Lett. 2025, 16, 6627−6636

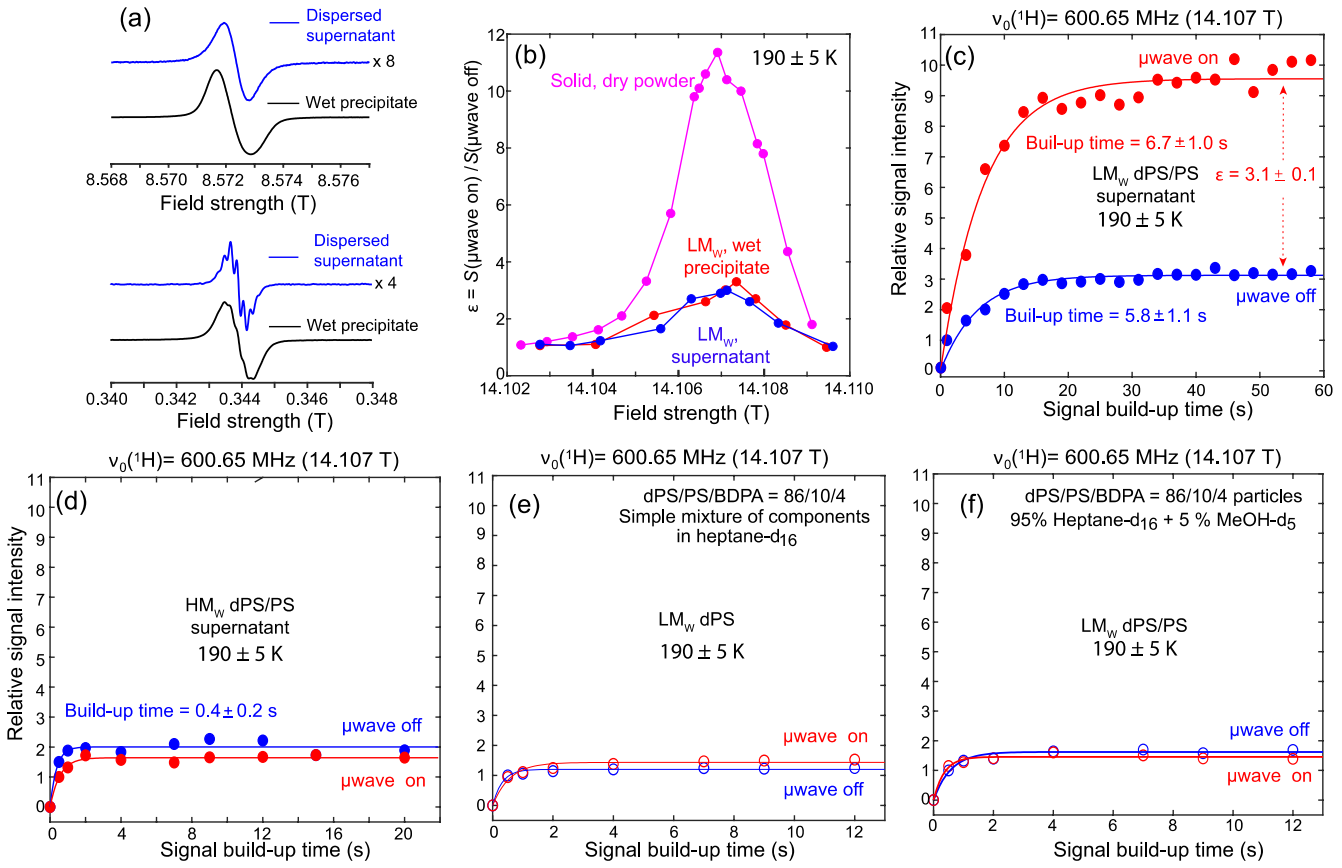

Figure 2. (a) EPR spectra of a LM_W dPS sample (dPS/PS/BDPA = 86.4/9.6/3.8 in weight ratio) measured at room temperature at 240 and 9.7 (X-band) GHz, in wet precipitates (black) and supernatant (blue) of the fine powders dispersed in *n*-hexane. (b) PM-DNP enhancement profiles obtained for the LM_W sample around the OE position for both supernatant (blue) and wet precipitates (red) in heptane-d_{16}, as well as for the LM_W dPS powder (pink). Blue and red profiles were generated by plotting the intensity ratios measured for the residual ^{1}Hs in liquid heptane-d_{16} in the presence or absence of microwaves, while varying the magnetic field (and ^{1}H Larmor frequency) around the central OE position. Build-up time = 15 s; d_1 = 60 s. (c) ^{1}H DNP build-up curves obtained for the residual ^{1}Hs in liquid heptane-d_{16} as driven by dispersed BDPA-doped dPS/PS LM_W particles, observed by toggling the microwave irradiation on (red) and off (blue) over a duration of up to 60 s (d_1 = 80 s, 190 K, MAS rate ν_r = 700 Hz). (d)−(f) Measurements conducted under the same conditions as in (c), but for the indicated samples. No OE DNP enhancement was observed in any of these cases for the ^{1}H spectrum of the residual solution-phase heptane.

measurements to assess sizes, according to their different sensitivities.

Figure 2b presents field sweep profiles recorded around the OE DNP position for the solution NMR signals emanating from supernatant (blue) and wet precipitate (red) samples obtained from the LM_W PS preparation. These profiles reflect the intensity ratios of ^{1}H NMR spectra measured at ∼190 K with μwave irradiation on and off, for the residual ^{1}Hs in the liquid heptane-d_{16} used to suspend the PS particles. Although the relative DNP enhancements of these integrated ^{1}H liquid spectra are smaller than the enhancements originating in the dPS/PS/BDPA powder itself (pink), the frequency-dependent features of their sweep profiles coincide with those of the solid sample. This suggests that it is the dPS/PS/BDPA particles dispersed in the heptane that are generating the DNP-driven enhancement of the latter's protons and that no significant μwave-derived thermal heating effects, which should be independent of the minor field changes here involved, are biasing these experiments. Figure 2c shows the ^{1}H particle-mediated DNP build-up curve observed for the heptane protons in the supernatant LM_W dPS/PS/BDPA sample, taken at the optimal OE position (600.65 MHz) and at a (calibrated) sample temperature of ≈190 K, while spinning the rotor at ν_r = 700 Hz (see Experimental Section and Supporting Information Section 4 for further technical details). The observed μwave-driven enhancement ε = 3.1 ± 0.1 of the heptane over its μwave-off counterpart, while ca. one-quarter of the value observed for the dPS/PS/BDPA sample in the solid state, is quite clear. The build-up time of this liquid-state enhancement is also longer than that of the solid dPS/PS/BDPA protons: 5.8 s vs 1.4 s. This is all consistent with the solid-DNP → liquid cross-relaxation mechanism that had been hypothesized. The precise value of the enhancement observed in the heptane depended somewhat on the exact composition of this LM_W dPS/PS/BDPA mix, but in general was maximum when PS was present in ca. 10% (Supporting Information, Section 5).

As illustrated in the Figure 2's remaining panels, no similar enhancements were detected for other assayed formulations. The HM_W PS sample, which gave a better enhancement than the LM_W counterpart in the solid state, did not enhance heptane in the supernatant phase at 190 K (Figure 2d). We speculate that this could be due to an inefficient cross-relaxation between the HM_W solid and the liquid protons, and/or due to the fact that the ^{1}H T_1 times in this liquid were too short for supporting a substantial cross-relaxation-derived buildup: indeed, the theoretical model further developed

https://doi.org/10.1021/acs.jpclett.5c01398
J. Phys. Chem. Lett. 2025, 16, 6627−6636

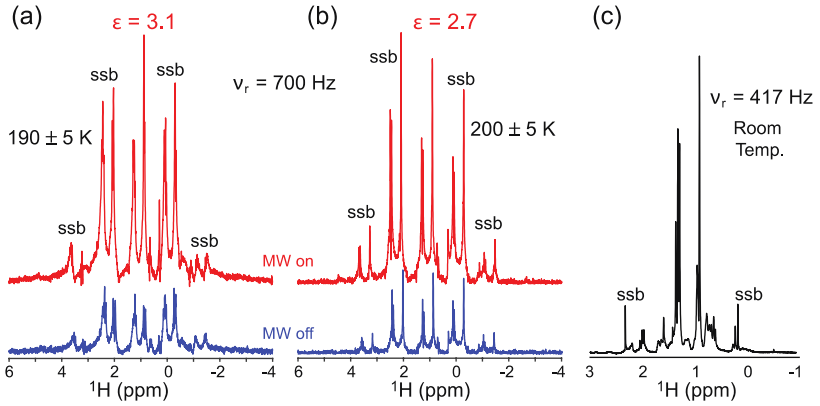

Figure 3. (a, b) Liquid-state ^{1}H NMR spectra LM_W dPS/PS/BDPA (86.4/9.6/3.8 wt %) dispersed in heptane-d_{16} recorded with microwaves on (red) and off (blue), obtained at the indicated temperatures and conditions, and leading to the indicated PM-DNP enhancement factors. These enhancements arose after a signal build-up time of 15 s and a delay time (d1) of 80 s. Spectra were collected using the echo sequence described in Figure 1 (2 scans; τ_1 = 250 us; τ_2 = 0 us). (c) ^{1}H NMR spectrum of heptane-d_{16} recorded at the indicated conditions. In all cases peak line widths were 1−2 Hz; ssb denotes spinning sidebands.

below would predict negligible PM-DNP enhancements for liquids that like this one, have $T_1 \approx 0.5$ s. Also important, no DNP enhancement was observed when other formulations containing LM_W dPS, PS and BDPA in a state that did not involve the suspended doped particles were assayed: Controls involving a mixture of dPS, PS and BDPA independently dissolved in heptane-d_{16} showed no effects upon μwave irradiation (Figure 2e), neither did a mixture of the particles suspended in heptane with a small percentage of methanol, which is a known PS dispersant leading to a "jelly-like" state (Figure 2f). This confirms a need for dispersed PS particles that are not dissolved in the solvent but can still interact intimately with it, perhaps also through a swelling of the polymer matrix, for the solid → solution chain of enhancing events to take place. The absence of a direct OE DNP effect on these samples also confirms that the enhancements observed are not artifacts associated with a heating of the sample, as driven by absorption of the μwave radiation by the solvent or radical.

Figure 3 panels a and b present examples of the ^{1}H NMR spectra that gave the origin to the data in Figure 2. These spectra were recorded for the heptane in the supernatant samples, for μwave on and off conditions at 190 and 200 K. Being mostly deuterated and therefore devoid from homonuclear J-couplings, these spectra should exhibit sharp singlets at 0.86 (single methyl peak) and 1.26−1.27 ppm (up to three methylene peaks). Singlet-like peaks are indeed observed in the μwave on/off spectra, exhibiting narrow peak widths at half heights (1−2 Hz) as expected from an isotropic liquid. Supporting Section 6 illustrates additional examples of these PM-DNP enhanced ^{1}H NMR experiments but for different polymer/radical compositions. A most evident feature of all these spectra is the presence of strong spinning sidebands, that repeat heptane's singlets structure at multiples of the MAS rate. These phenomena are not reflective of solid anisotropies, but rather of susceptibility and rf inhomogeneity issues associated with the probe that was used;[57,58] they were not associated with any sample composition and were also observed in neat heptane (Figure 3c) or even in water samples (Supporting Information, Section 7). These sidebands eventually span away at rates >2−3 kHz and are thus not usually observed in solid state MAS DNP experiments carried out at these or higher spinning rates. However, in the present case, spinning the rotor containing the supernatant sample at rates exceeding a few 100 Hz led to centrifugation of the dispersed dPS/PS/BDPA particles and to elimination of the observed liquid-state DNP enhancements. On the other hand, static sample experiments led to broad, ca. 1 ppm line widths, depriving the resulting spectra from a liquid-like character (Supporting Information, Figure S7). Consequently, experiments had to be conducted at the slowest possible rotation rates, which while leading to excellent resolution, were also accompanied by these sideband artifacts.

The PM-DNP experiment hereby presented was proposed based on a relayed BDPA → PS(solid) → Heptane(liquid) transfer process. As the characteristics of each individual polarization-transfer process in this chain can be independently measured, it should be in principle possible to check consistency between the overall enhancements and buildup time scales shown in Figures 2 and 3 and each step's independent observables. Doing so requires, in turn, a theoretical framework linking the two sets of measurements. To this effect the cross-relaxation between the ^{1}Hs of the PS (solid S) and those of the heptane (liquid L) were described as in terms of their enhancements ε over (in principle identical) thermal polarization values S_0 and L_0, $\varepsilon_S = S/S_0$ and $\varepsilon_L = L/L_0$. Starting from a DNP-enhanced set of Solomon equations linking these two phases, we can connect these enhancements as done in ref 50:

$$\frac{d\varepsilon_S}{dt} = B_S\left(\frac{P_e}{P_S} - \varepsilon_s\right) - R_S(\varepsilon_S - 1) - \sigma_{SL}(\varepsilon_L - 1) \quad (1)$$

$$\frac{d\varepsilon_L}{dt} = -R_L(\varepsilon_L - 1) - \sigma_{LS}(\varepsilon_S - 1) \quad (2)$$

Here B_S is the buildup rate constant for the ^{1}H nucleus of the PS solid, brought about by a P_e electron radical polarization enhancing the P_S polarization of the PS ^{1}Hs; $R_{S/L}$ are the self-relaxation rates $(1/T_1)$ of the solid and liquid protons, and the σ's denote the cross-relaxation rates between the two reservoirs. The ratio $P_e/P_S = \varepsilon_S^0$ corresponds to the maximum efficiency that the μwave-driven OE DNP process will impart on the solid protons and is in essence the final ^{1}H DNP solid-state polarization enhancement described experimentally in Figure 1c. Assuming for simplicity that this effect is much

https://doi.org/10.1021/acs.jpclett.5c01398
J. Phys. Chem. Lett. 2025, 16, 6627−6636

larger than the $\sigma_{SL}(\varepsilon_S - 1)$ losses due to polarization transfers to the solvent protons, the latter term can be disregarded and integration of eq 1 for the boundary condition $\varepsilon_S = 0$ at $t = 0$ yields

$$\varepsilon_S = \frac{B_S\varepsilon_S^0 + R_S}{(B_S + R_S)}\{1 - \exp[-(B_{ps} + R_{ps})t]\} \quad (3)$$

Inserting this into eq 2 and integrating yields an analytical expression for the time-dependent enhancement being transferred to the liquid-state protons (see Supporting Information, Section 8):

$$\varepsilon_L(t) = \frac{a}{R_L} + \frac{c}{R_L - c}e^{-ct} + \left(1 - \frac{a}{R_L} - \frac{b}{R_L - c}\right)e^{-R_L t} \quad (4)$$

where $a = R_L + \sigma_{LS} + \sigma_{SL}\left(\frac{B_S\varepsilon_S^0 + R_S}{(B_S + R_S)}\right)$, $b = -\sigma_{LS}\left(\frac{B_S\varepsilon_S^0 + R_S}{(B_S + R_S)}\right)$, and $c = B_S + R_S$.

Several of the parameters involved in this equation, including the solids buildup rate and individual longitudinal relaxation rates, can and were measured in independent experiments: Figures 1 and 2 provide estimates for the relaxation and DNP buildup rates and maximal enhancements in the solid, Supporting Information Section 9 describes the saturation transfer difference (STD) measurements yielding the polymer → heptane-d_{16} cross-relaxation rates, and Supporting Information Section 10 presents the ancillary liquid state relaxation data. These yielded nearly identical 0.94 s relaxation times for the CDH and CD_2H resonances in neat heptane-d_{16} and longer values 4.5 and 7.6 s, respectively, for these sites in the presence of the dPS/PS/BDPA polarizing particles. Figure 4 shows a fit of the ensuing liquid-state experimental PM-DNP enhancements to eq 4, plotted as a function of the μwave irradiation time. Assuming again a negligible $\sigma_{LS} = 0$ value, one can see that neither the average heptane-d_{16} T_1 values in the presence (5.8 s, magenta line in Figure 4) nor in the absence (1 s, black line) of the polarizing particles provide a perfect fit for the buildup data. An intermediate T_1 value of 2.6 s, however, quantitatively recapitulates the liquid buildup behavior. We believe that this reflects the fact that the heptane-d_{16} T_1 values that matter in the calculation of the liquid-state DNP enhancement are derived from protons at the particle/liquid interface, whose relaxation properties are probably different from the ones measured by any bulk-based technique. When considering that, in addition, the R_S values measured probably also reflect the bulk of the PS rather than the relevant protons at the PS/heptane interface, that the PS enhancement values ε_S^0 were measured in the absence of the organic solvent, and that a number of approximations were taken (e.g., negligible polarization losses of the solid ^{1}H polarization by the transfer to the liquid ^{1}Hs, negligible liquid → solid polarization back-transfers), it is fair to say that the independent measurements and the aforementioned model reproduce satisfactorily the behavior in the liquid-state PM-DNP spectra.

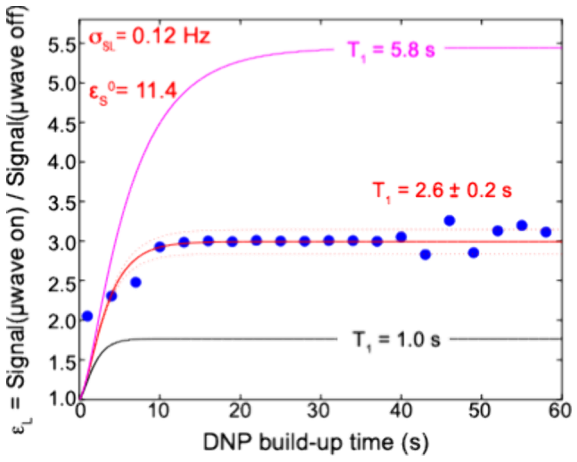

Figure 4. Fitting the experimental DNP-enhanced buildup data for heptane-d_{16}, according to the multistep BDPA → PS(solid) → Heptane(liquid) polarization transfer mechanism presented in the text. A common (average) enhancement ε_L was taken for both methyl and methylene protons. Blue dots represent the experimentally obtained ε_L values calculated at each build-up time point; the solid red line represents the best-fit of eq 4 for σ_{SL} = 0.12 Hz, ε_S^0 = 11.4, T_1(S) = 1.5 s, B_S(PS) = 0.5 s^{-1}, T_1(heptane) = 2.6 s. Dashed red lines indicate error bounds for ± 0.2 s; magenta and black lines indicate the behaviors expected for the indicated T_1(L) values.

A final feature worth discussing is the ca. 10-fold longer build-up time exhibited by the polarizing liquid in the low-M_w sample experiment in Figure 2b, vs the subsecond T_1 build-up times evidenced by the nonpolarizing conditions in Figure 2c–f. To shed light on this, ^{1}H T_1 values were measured at 190 K on pure heptane-d_{16}, and on a low-M_W sample optimized for the DNP experiment (heptane-d_{16} with dispersed dPS/PS/BDPA 86.5/9.6/3.9 wt % microparticles; see Supporting Information, Section 10). Once again, the liquid-state T_1 relaxation times of these two samples differ significantly. In pure heptane-d_{16} the T_1 values for both the methylene and methyl moieties were 0.94 ± 0.04 s—comparable to the build-up times in Figure 2c–f. By contrast, T_1 values for the DNP-enhancing sample were substantially longer and akin to those measured in Figure 2b: 4.5 ± 0.4 and 7.6 ± 0.9 s for the methylene and methyl groups, respectively. These increases in T_1 values induced by the dispersed microparticles, which might arise from viscosity changes but whose origin remains to be elucidated, facilitate in turn the cross-relaxation between ^{1}H(PS) on the particles' surfaces and ^{1}H(heptane) in the liquid phase, and may be responsible for the differential DNP behaviors shown in Figure 2. Indeed, in all samples whose solution relaxation times T_1 were short and similar to those observed in pure heptane-d_{16}, no significant DNP effects built up by the relatively slow ($\sigma_{SL} \approx 0.12$ Hz) solid → liquid cross-relaxation rate. Further reduction of the T_1(L)*σ_{SL} product most likely are also responsible for the negligible PM-DNP enhancements observed when $T \geq 200$ K (Supporting Information, Section 11).

In a search for the elusive goal of achieving ^{1}H DNP enhancements on solution-state samples approaching the normal volumes used in analytical NMR, this study explored an indirect route based on e^- → solid-^{1}Hs → liquid-^{1}Hs particle-mediated DNP transfers. Doped PS was here chosen as the polarizing particles because of their ability to undergo DNP outside cryogenic regimes, which will usually be incompatible with solution state investigations. Organic solvents on the other hand can remain fluid over a range of temperatures, and hence, liquid-state organic NMR is not necessarily synonymous with room-temperature DNP NMR. As shown in the Supporting Information (Section 11), the solution NMR enhancements here achieved are in fact highly temperature dependent: Figure S11 shows that repeating the experiment

https://doi.org/10.1021/acs.jpclett.5c01398
J. Phys. Chem. Lett. 2025, 16, 6627–6636

illustrated in Figure 2c (190 K) using an identical sample and conditions other than for slightly lower (185 K) or higher (220 K) temperatures leads to noticeably higher or lower enhancements, respectively. A full characterization of these effects thus calls for careful measurements of the μwave on/off influence on sample temperature, which were here accounted for by the calibrations described in the Supporting Information, Section 4. In this respect, it was noticed that working at temperatures $\leq$180 K that are close to the heptane/PS freezing point risked changing the mobility of the heptane molecules, and hence their ^{1}H NMR spectrum, by microwave irradiation—even when working off the OE condition. Temperatures at the melting point interface, however, were also accompanied by a merging of the multiple ^{1}H heptane peaks into a single broader peak; these spectral changes were very evident and helped to avoid confounding factors.

The experiments here presented are still a distance away from practical analytical applications: the enhancements imparted by PM-DNP are still modest, the spinning sideband patterns are an annoyance, and enhancements of codissolved solutes remain to be tested. On the other hand, the solids DNP/liquid cross-relaxation mechanism appears general and open to several potential improvements. Extensive optimizations in the formulation, the hardware, and the conditions that can be assessed in this kind of experiment remain to be carried out. And while liquid-state high-field DNP investigations on samples in the 10−100 μL range are likely to be unfeasible in aqueous phases because of microwave penetration problems, it is worth remembering that most analytical NMR work still takes place in organic liquids. Hence, further progress in the PM-DNP area appears to be well worth the effort.

EXPERIMENTAL SECTION

Chemicals. Low molecular weight (LM_W) deuterated polystyrene-d_8 (dPS; M_W = 2.23 kDa, 98% D) and high molecular weight (HM_W) dPS (M_W = 412 kDa) were purchased from Cambridge Isotope Laboratories and Polymer Source, Inc. (Quebec, Canada), respectively. Nondeuterated polystyrene (PS; M_W = 280 kDa) was obtained from Aldrich. Perdeuterated heptane-d_{16} (99 atom % D), methanol-d_5 (99.8 atom % D), toluene, and BDPA (1,3-bis[diphenylene]-2-phenylallyl) free radical (1:1 complex with benzene) were all purchased from Sigma-Aldrich and used as received. All solvents were deoxygenated by undergoing at least five freeze−degassing−purge (N_2)−thaw cycles and were stored in a glovebox with a tight seal.

Production of BDPA-Doped dPS/PS Powder Samples. 60.0 mg of dPS, 6.7 mg of PS, and 2.8 mg of BDPA were placed in a 7.5 mL glass vial with a magnetic stirring bar. Approximately 200 μL of toluene was added. The target composition corresponds to doping about 4% BDPA into a polymer matrix consisting of 90% dPS and 10% PS, with the relative weight ratio of the components being dPS/PS/BDPA = 86.4/9.6/4.0. The mixture was stirred for about 2 h on a magnetic stirrer until it dissolved completely and homogeneously. The resulting solution was poured onto a glass plate to form polymer films, allowing toluene to evaporate at room temperature. To make the solid film more brittle and easier to grind into micropowders, the remaining toluene was removed using a vacuum oven without heating. Thin films of BDPA-doped dPS/PS samples recovered from glass plates after solvent evaporation were converted into microparticles by ball milling. Ball milling was performed to reduce the particle size using a Retsch Mixer Mill 400. The process utilized two 10 mL stainless steel jars, each containing six 3 mm stainless steel bearings, operated at a milling frequency of 30 Hz for a total of 1 h. Prior to milling, the jars with the samples and bearings were submerged in liquid nitrogen until vigorous boiling subsided (approximately 10−15 min). After every 10 min of milling, the jars were resubmerged in liquid nitrogen for around 5 min until boiling subsided, repeating this process until the 1 h milling time was complete. The low temperatures and use of numerous small bearings aimed to further minimize particle size.[59,60] The ball-milled BDPA-doped dPS/PS powder samples were kept in a glovebox to remove any oxygen trapped in the solid matrix. Supporting Information describes how these samples were readied for the DNP NMR measurements.

NMR Experiments. The 90° pulse lengths for ^{1}H, ^{13}C, and ^{79}Br were 2.5 μs, 5 μs, and 5 μs, respectively. ^{1}H NMR spectra were acquired by coadding two scans with an acquisition delay time of d_1 = 60−80 s and a MAS rate ν_r = 200−700 Hz, while alternating the phases of both the 180° pulse and signal receiver between 0 and π. The echo delay times in the Hahn echo sequence were set to 250 μs before and 1 μs after the 180° pulse to preserve the early portion of the signal. For the ^{1}H−^{13}C CPMAS experiments carried out on the solid BDPA-doped dPS/PS powders, the parameters used were ν (^{1}H) = 55 kHz and ν (^{13}C) = 50 kHz for 1 ms for the CP mixing by employing a ramped (90%−110%) spin-lock pulses along the ^{1}H channel. The ^{1}H decoupling power used for the ^{13}C detection was about 90 kHz while employing the SPINAL-64 sequence.[55] The MAS rate used for the ^{1}H−^{13}C CPMAS experiment was about ν_r = 5 kHz. A 90° read pulse was applied after the saturation recovery sequence and a variable delay time to measure ^{79}Br T_1 for temperature calibration.[61]

DNP Experiments. ^{1}H MAS DNP NMR spectra were acquired from the liquid heptane-d_{16} (ca. 99 % D) solution that is dispersed with BDPA-doped dPS/PS micropowders. These spectra were acquired using a widebore ^{1}H 600 MHz Bruker Avance III spectrometer configured to a 395 GHz gyrotron microwave source and a Bruker 3.2 mm MAS ^{1}H-X-Y triple-resonance probe. Approximately 30 μL of heptane-d_{16}/dPS/PS/BDPA colloidal solution was filled into a 3.2 mm sapphire MAS rotor with a silicon rubber septum and a Vespel polyimide cap. The MAS spinning rate employed in the experiments was in the range of 200−700 Hz, while cooling the sample compartment to 185−200 K using a nitrogen gas stream evaporated from a liquid nitrogen tower. Approximately 13 W microwave power from the gyrotron source via the optic table was fed into the sample from the probe base. Microwave irradiation was applied to the sample rotor only during the signal build-up time that follows right after the signal saturation sequence, [90° (^{1}H) pulse-1 ms delay]$_n$ ($n \approx 50$), while it was turned off during other parts of the sequence including the recycle delay time (d_1). Microwave control was managed by opening and closing a shutter using TTL signals, precisely synchronized with the start and end of the signal build-up time in the pulse sequence. This ensured accurate on−off switching and optimized microwave usage by minimizing unnecessary irradiation during periods when it was not needed. The saturation recovery sequence was employed in all our sequences used in the experiments, including the ^{1}H DNP NMR experiments, ^{1}H-enhanced ^{1}H−^{13}C CPMAS experiments as well as ^{79}Br T_1 measurements (along ^{79}Br) for temperature calibration.

https://doi.org/10.1021/acs.jpclett.5c01398
J. Phys. Chem. Lett. 2025, 16, 6627−6636

All of the graphs in the main and supporting texts, along with the associated error ranges, were constructed and analyzed by using the curve fitting toolbox provided by the Matlab software.

■ ASSOCIATED CONTENT

Supporting Information

The Supporting Information is available free of charge at https://pubs.acs.org/doi/10.1021/acs.jpclett.5c01398.

Additional details on the NMR, EPR and dynamic light scattering measurements; self- and cross-relaxation rates; temperature and sample dependencies of the PM-DNP enhancement; nature of the spinning sidebands; full description of the PM-DNP mechanism and kinetic modeling (PDF)

■ AUTHOR INFORMATION

Corresponding Authors

Sungsool Wi − *National High Magnetic Field Laboratory, Tallahassee, Florida 32304, United States*; Email: sungsool@magnet.fsu.edu

Lucio Frydman − *National High Magnetic Field Laboratory, Tallahassee, Florida 32304, United States; Department of Chemical and Biological Physics, Weizmann Institute of Science, 7610001 Rehovot, Israel*; orcid.org/0000-0001-8208-3521; Email: lucio.frydman@weizmann.ac.il

Authors

Angeliki Giannouli − *Department of Chemical and Biological Physics, Weizmann Institute of Science, 7610001 Rehovot, Israel;* Present Address: Department of Chemistry, University of Crete, Heraklion 70013, Greece; orcid.org/0000-0001-8017-5457

Korin Butbul − *Department of Chemical and Biological Physics, Weizmann Institute of Science, 7610001 Rehovot, Israel*

Jenica Lumata − *National High Magnetic Field Laboratory, Tallahassee, Florida 32304, United States;* orcid.org/0000-0002-4650-3768

Thierry Dubroca − *National High Magnetic Field Laboratory, Tallahassee, Florida 32304, United States*

Faith Scott − *National High Magnetic Field Laboratory, Tallahassee, Florida 32304, United States;* orcid.org/0000-0003-3903-8842

Zachary Dowdell − *Department of Chemistry and Biochemistry, Florida State University, Tallahassee, Florida 32306, United States*

Robert W. Schurko − *National High Magnetic Field Laboratory, Tallahassee, Florida 32304, United States; Department of Chemistry and Biochemistry, Florida State University, Tallahassee, Florida 32306, United States;* orcid.org/0000-0002-5093-400X

Hans Van Tol − *National High Magnetic Field Laboratory, Tallahassee, Florida 32304, United States;* orcid.org/0000-0001-6972-2149

Complete contact information is available at: https://pubs.acs.org/10.1021/acs.jpclett.5c01398

Notes

The authors declare no competing financial interest.

■ ACKNOWLEDGMENTS

We thank Drs. Stephen Hill and Frederic Mentink-Vigier for valuable discussions. This work was mostly performed at the National High Magnetic Field Laboratory, which is supported by National Science Foundation Cooperative Agreement No. DMR-2128556 and the State of Florida. The MAS-DNP instrument is supported by NIH P41 GM122698 and NIH RM1-GM148766. S.W. and J.L. acknowledge support from the National Science Foundation (Grant No. CHE-2203405). R.W.S. and Z.D. thank the Florida State University, National High Magnetic Field Laboratory, and the State of Florida for funding this research. Supports from the Israel Science Foundation (grant 1874/22) and the Perlman Family Foundation are gratefully acknowledged by L.F.

■ REFERENCES

(1) Abragam, A. *Principles of Nuclear Magnetism*; Oxford University Press: Oxford, 1961.

(2) Ernst, R. R.; Bodenhausen, G.; Wokaun, A. *Principles of Nuclear Magnetic Resonance in one and two dimensions*; Oxford University Press: New York, 1987.

(3) Cavanagh, J.; Fairbrother, W. J.; Palmer, A. G., III; Rance, M.; Skelton, N. J. *Protein NMR Spectroscopy: Principles and Practice*; Academic Press, 1995.

(4) Wuthrich, K. *NMR of Proteins and Nucleic Acids*; John Wiley & Sons: New York, 1986.

(5) Overhauser, A. W. Polarization of Nuclei in Metals. *Phys. Rev.* **1953**, *92* (2), 411−415.

(6) Carver, T.; Slichter, C. P. Polarization of Nuclear Spins in Metals. *Phys. Rev.* **1953**, *92*, 212−213.

(7) Carver, T. R.; Slichter, C. P. Experimental Verification of the Overhauser Nuclear Polarization Effect. *Phys. Rev.* **1956**, *102*, 975−980.

(8) Maly, T.; Debelouchina, G. T.; Bajaj, V. S.; Hu, K. N.; Joo, C. G.; Mak-Jurkauskas, M. L.; Sirigiri, J. R.; Van Der Wel, P. C. A.; Herzfeld, J.; Temkin, R. J.; Griffin, R. G. Dynamic Nuclear Polarization at High Magnetic Fields. *J. Chem. Phys.* **2008**, *128*, 052211.

(9) Ni, Q. Z.; Daviso, E.; Can, T. V.; Markhasin, E.; Jawla, S. K.; Swager, T. M.; Temkin, R. J.; Herzfeld, J.; Griffin, R. G. High Frequency Dynamic Nuclear Polarization. *Accounts Che. Res.* **2013**, *46* (9), 1933−1941.

(10) Michaelis, V., Griffin, R., Corzilius, B., Vega, S., Eds. *Handbook of High Field Dynamic Nuclear Polarization*; Wiley Ltd., 2020.

(11) Liao, W.-C.; Ong, T.-C.; Gajan, D.; Bernada, F.; Sauvée, C.; Yulikov, M.; Pucino, M.; Schowner, R.; Schwarzwälder, M.; Buchmeiser, M. R.; Jeschke, G.; Tordo, P.; Ouari, O.; Lesage, A.; Emsley, L.; Copéret, C. Dendritic polarizing agents for DNP SENS. *Chem. Sci.* **2017**, *8*, 416−422.

(12) Hausser, K. H.; Stehlik, D. Dynamic Nuclear Polarization in Liquids. *Adv. Magn. Reson.* **1968**, *3*, 79.

(13) Dwek, R. A.; Richards, R. E.; Taylor, D. Nuclear Electron Double Resonance in Liquids. *Annu. Rep. NMR Spectrosc.* **1969**, *2*, 293−344.

(14) Gitti, R.; Wild, C.; Tsiao, C.; Zimmer, K.; Glass, T. E.; Dorn, H. C. Solid-Liquid Intermolecular Transfer of Dynamic Nuclear Polarization. Enhanced Flowing Fluid ^{1}H NMR Signals via Immobilized Spin Labels. *J. Am. Chem. Soc.* **1988**, *110*, 2294−2296.

(15) Muller-Warmuth, W.; Meise-Gresch, K. Molecular motions and interactions as studied by dynamic nuclear polarization (DNP) in free radical solutions. *Adv. Magn. Reson.* **1983**, *11*, 1−45.

(16) Ardenkjaer-Larsen, J. H.; Fridlund, F.; Gram, A.; Hansson, G.; Hansson, L.; Lerche, M. H.; Servin, R.; Thaning, M.; Golman, K. Increase in signal-to-noise ratio of > 10,000 times in liquid-state NMR. *Proc. Natl. Acad. Sci. U.S.A.* **2003**, *100*, 10158−10163.

(17) Armstrong, B. D.; Han, S. A new model for Overhauser enhanced nuclear magnetic resonance using nitroxide radicals. *J. Chem. Phys.* **2007**, *127*, 104508.

(18) Lingwood, M. D.; Han, S. Chapter 3 - Solution-State Dynamic Nuclear Polarization. *Annu. Rep. NMR Spectrosc.* **2011**, *73*, 83−126.
(19) Brindle, K. M.; Bohndiek, S. E.; Gallagher, F. A.; Kettunen, M. I. Tumor imaging using hyperpolarized 13C magnetic resonance spectroscopy. *Magn. Reson. Med.* **2011**, *66*, 505−519.
(20) Nelson, S. J.; Vigneron, D.; Kurhanewicz, J.; Chen, A.; Bok, R.; Hurd, R. DNP-Hyperpolarized 13C Magnetic Resonance Metabolic Imaging for Cancer Applications. *Appl. Magn. Reson.* **2008**, *34*, 533−544.
(21) Kurhanewicz, J.; Vigneron, D. B.; Brindle, K.; Chekmenev, E. Y.; Comment, A.; Cunningham, C. H.; DeBerardinis, R. J.; Green, G. G.; Leach, M. O.; Rajan, S. S.; Rizi, R. R.; Ross, B. D.; Warren, W. S.; Malloy, C. R. Analysis of Cancer Metabolism by Imaging Hyperpolarized Nuclei: Prospects for Translation to Clinical Research. *Neoplasia* **2011**, *13*, 81−97.
(22) Harris, T.; Bretschneider, C.; Frydman, L. Dissolution DNP NMR with solvent mixtures: Substrate concentration and radical extraction. *J. Magn. Reson.* **2011**, *211*, 96−100.
(23) Bornet, A.; Melzi, R.; Perez Linde, A. J.; Hautle, P.; van den Brandt, B.; Jannin, S.; Bodenhausen, G. Boosting Dissolution Dynamic Nuclear Polarization by Cross Polarization. *Phys. Chem. Lett.* **2013**, *4*, 111−114.
(24) Hilty, C.; Kurzbach, D.; Frydman, L. Hyperpolarized Water as Universal Sensitivity Booster in Biomolecular NMR. *Nat. Protoc.* **2022**, *17*, 1621−1657.
(25) Bowen, S.; Hilty, C. Rapid sample injection for hyperpolarized NMR spectroscopy. *Phys. Chem. Chem. Phys.* **2010**, *12*, 5766−5770.
(26) Reese, M.; Lennartz, D.; Marquardsen, T.; Höfer, P.; Tavernier, A.; Carl, P.; Schippmann, T.; Bennati, M.; Carlomagno, T.; Engelke, F.; Griesinger, C. Construction of a Liquid-State NMR DNP Shuttle Spectrometer: First Experimental Results and Evaluation of Optimal Performance Characteristics. *Appl. Magn. Reson.* **2008**, *34*, 301−311.
(27) Höfer, P.; Parigi, G.; Luchinat, C.; Carl, P.; Guthausen, G.; Reese, M.; Carlomagno, T.; Griesinger, C.; Bennati, M. Field Dependent Dynamic Nuclear Polarization with Radicals in Aqueous Solution. *J. Am. Chem. Soc.* **2008**, *130*, 3254−3255.
(28) van Meerten, S. G. J.; Tayler, M. D. C.; Kentgens, A. P. M.; van Bentum, P. J. M. Towards Overhauser DNP in supercritical CO2. *J. Magn. Reson.* **2016**, *267*, 30−36.
(29) Joo, C.-G.; Hu, K.-N.; Bryant, J. A.; Griffin, R. G. In Situ Temperature Jump High-Frequency Dynamic Nuclear Polarization Experiments: Enhanced Sensitivity in Liquid-State NMR Spectroscopy. *J. Am. Chem. Soc.* **2006**, *128*, 9428−9432.
(30) Leggett, M. S. J.; Hunter, R.; Granwehr, J.; Panek, R.; Perez-Linde, A. J.; Horsewill, A. J.; McMaster, J.; Smith, G.; Köckenberger, W. A dedicated spectrometer for dissolution DNP NMR spectroscopy. *Phys. Chem. Chem. Phys.* **2010**, *12*, 5883−5892.
(31) Sharma, M.; Janssen, G.; Leggett, J.; Kentgens, A. P. M.; van Bentum, P. J. M. Rapid-melt Dynamic Nuclear Polarization. *J. Magn. Reson.* **2015**, *258*, 40−48.
(32) Yoon, D.; Soundararajan, M.; Caspers, C.; Braunmueller, F.; Genoud, J.; Alberti, S.; Ansermet, J.-P. J. 500-fold enhancement of in situ 13C liquid state NMR using gyrotron-driven temperature-jump DNP. *J. Magn. Reson.* **2016**, *270*, 142−146.
(33) Grazia Concilio, M.; Frydman, L. Steady state effects introduced by local relaxation modes on J-driven DNP-enhanced NMR. *J. Magn. Reson.* **2023**, *355*, 107542.
(34) Concilio, M. G.; Frydman, L. Microwave-free *J*-driven dynamic nuclear polarization: A proposal for enhancing the sensitivity of solution-state NMR. *Phys. Rev. E* **2023**, *107*, 35303.
(35) Villanueva-Garibay, J. A.; Annino, G.; van Bentum, P. J. M.; Kentgens, A. P. M. Pushing the limit of liquid-state dynamic nuclear polarization at high field. *Phys. Chem. Chem. Phys.* **2010**, *12* (22), 5846−5849.
(36) Kryukov, E. V.; Pike, K. J.; Tam, T. K. Y.; Newton, M. E.; Smith, M. E.; Dupree, R. Determination of the temperature dependence of the dynamic nuclear polarisation enhancement of water protons at 3.4 T. *Phys. Chem. Chem. Phys.* **2011**, *13*, 4372−4380.
(37) van Bentum, P. J. M.; van der Heijden, G. H. A.; Villanueva-Garibay, J. A.; Kentgens, A. P. M. Quantitative analysis of high field liquid state dynamic nuclear polarization. *Phys. Chem. Chem. Phys.* **2011**, *13*, 17831−17840.
(38) Liu, G.; Levien, M.; Karschin, N.; Parigi, G.; Luchinat, C.; Bennati, M. One-thousand-fold enhancement of high field liquid nuclear magnetic resonance signals at room temperature. *Nat. Chem.* **2017**, *9*, 676−680.
(39) Loening, N. M.; Rosay, M.; Weis, V.; Griffin, R. G. Solution-State Dynamic Nuclear Polarization at High Magnetic Field. *J. Am. Chem. Soc.* **2002**, *124*, 8808−8809.
(40) Bennati, M.; Luchinat, C.; Parigi, G.; Turke, M.-T. Water 1H relaxation dispersion analysis on a nitroxide radical provides information on the maximal signal enhancement in Overhauser dynamic nuclear polarization experiments. *Phys. Chem. Chem. Phys.* **2010**, *12*, 5902−5910.
(41) Levien, M.; Yang, L.; van der Ham, A.; Reinhard, M.; John, M.; Purea, A.; Ganz, J.; Marquardsen, T.; Tkach, I.; Orlando, T.; Bennati, M. Overhauser enhanced liquid state nuclear magnetic resonance spectroscopy in one and two dimensions. *Nat. Commun.* **2024**, *15*, 5904.
(42) Neugebauer, P.; Krummenacker, J. G.; Denysenkov, V. P.; Helmling, C.; Luchinat, C.; Parigi, G.; Prisner, T. F. High-field liquid state NMR hyperpolarization: a combined DNP/NMRD approach. *Phys. Chem. Chem. Phys.* **2014**, *16* (35), 18781−18787.
(43) Kuzhelev, A. A.; Denysenkov, V.; Ahmad, I. M.; Rogozhnikova, O. Y.; Trukhin, D. V.; Bagryanskaya, E. G.; Tormyshev, V. M.; Sigurdsson, S. T.; Prisner, T. F. Solid-Effect Dynamic Nuclear Polarization in Viscous Liquids at 9.4 T Using Narrow-Line Polarizing Agents. *J. Am. Chem. Soc.* **2023**, *145*, 10268−10274.
(44) Denysenkov, V.; Dai, D.; Prisner, T. F. A triple resonance (e, 1H, 13C) probehead for liquid-state DNP experiments at 9.4 T. *J. Magn. Reson.* **2022**, *337*, 107185.
(45) Kuzhelev, A.; Dai, D.; Denysenkov, V.; Prisner, T. Solid-like Dynamic Nuclear Polarization Observed in the Fluid Phase of Lipid Bilayers at 9.4 T. *J. Am. Chem. Soc.* **2022**, *144* (3), 1164−1168.
(46) Neugebauer, P.; Krummenacker, J. G.; Denysenkov, V. P.; Parigi, G.; Luchinat, C.; Prisner, T. F. Liquid state DNP of water at 9.2 T: an experimental access to saturation. *Phys. Chem. Chem. Phys.* **2013**, *15* (16), 6049−6056.
(47) Prandolini, M. J.; Denysenkov, V. P.; Gafurov, M.; Endeward, B.; Prisner, T. F. High-Field Dynamic Nuclear Polarization in Aqueous Solutions. *J. Am. Chem. Soc.* **2009**, *131*, 6090−6092.
(48) Denysenkov, V.; Prandolini, M. J.; Gafurov, M.; Sezer, D.; Endeward, B.; Prisner, T. F.; Denysenkov, V.; Prandolini, M. J.; Gafurov, M.; Sezer, D.; Endeward, B.; Prisner, T. F. Liquid state DNP using a 260 GHz high power gyrotron. *Phys. Chem. Chem. Phys.* **2010**, *12*, 5786−5790.
(49) Nishimura, K.; Kouno, H.; Tateishi, K.; Uesaka, T.; Ideta, K.; Kimizuka, N.; Yanai, N. Triplet Dynamic Nuclear Polarization of Nanocrystals Dispersed in Water at Room Temperature. *Phys. Chem. Chem. Phys.* **2019**, *21*, 16408−16412.
(50) Matsumoto, N.; Nishimura, K.; Kimizuka, N.; Nishiyama, Y.; Tateishi, K.; Uesaka, T.; Yanai, N. Proton Hyperpolarization Relay from Nanocrystals to Liquid Water. *J. Am. Chem. Soc.* **2022**, *144*, 18023−18029.
(51) Afeworki, M.; McKay, R. A.; Schaefer, J. Selective Observation of the Interface of Heterogeneous Polycarbonate/Polystyrene Blends by Dynamic Nuclear Polarization Carbon-13 NMR Spectroscopy. *Macromolecules* **1992**, *25*, 4084−4091.
(52) Wind, R. A.; Duijvestijn, M. J.; van der Lugt, C.; Manenschijn, A.; Vriend, J. Applications of Dynamic Nuclear Polarization in 13C NMR in Solids. *Prog. Nucl. Magn. Reson. Spectrosc.* **1985**, *17*, 33−67.
(53) Can, T. V.; Caporini, M. A.; Mentink-Vigier, F.; Corzilius, B.; Walish, J. J.; Rosay, M.; Maas, W. E.; Baldus, M.; Vega, S.; Swager, T. M.; Griffin, R. G. Overhauser Effects in Insulating Solids. *J. Chem. Phys.* **2014**, *141*, 064202.
(54) Ji, X.; Can, T.V.; Mentink-Vigier, F.; Bornet, A.; Milani, J.; Vuichoud, B.; Caporini, M.A.; Griffin, R.G.; Jannin, S.; Goldman, M.;

https://doi.org/10.1021/acs.jpclett.5c01398
J. Phys. Chem. Lett. 2025, 16, 6627−6636

Bodenhausen, G. Overhauser effects in non-conducting solids at 1.2 K. *J. Magn. Reson.* **2018**, *286*, 138−142.
(55) Fung, B.M.; Khitrin, A.K.; Ermolaev, K. An improved broadband decoupling sequence for liquid crystals and solids. *J. Magn. Reson.* **2000**, *142*, 97−101.
(56) Stoll, S.; Schweiger, A. EasySpin, a comprehensive software package for spectral simulation and analysis in EPR. *J. Magn. Reson.* **2006**, *178* (1), 42−55.
(57) Elbayed, K.; Dillmann, B.; Raya, J.; Piotto, M.; Engelke, F. Field modulation effects induced by sample spinning: application to high-resolution magic angle spinning NMR. *J. Magn. Reson.* **2005**, *174*, 2−26.
(58) Avni, R.; Mangoubi, O.; Bhattacharyya, R.; Degani, H.; Frydman, L. Magnetization Transfer Magic-Angle-Spinning z-Spectroscopy of Excised Tissues. *J. Magn. Reson.* **2009**, *199*, 1−9.
(59) Raghuraman, P.; Raman, R. R.; Pitchumani, B. Studies in Fine Grinding in an Attritor Mill. *Dev. Miner. Process.* **2000**, *13*, C4-94−C4-98.
(60) Shin, H.; Lee, S.; Jung, H. S.; Kim, J. B. Effect of Ball Size and Powder Loading on the Milling Efficiency of a Laboratory-Scale Wet Ball Mill. *Ceram. Int.* **2013**, *39*, 8963−8968.
(61) Thurber, K. R.; Tycko, R. Measurement of sample temperatures under magic-angle spinning from the chemical shift and spin-lattice relaxation rate of 79Br in KBr powder. *J. Magn. Reson.* **2009**, *196* (1), 84−87.

https://doi.org/10.1021/acs.jpclett.5c01398
J. Phys. Chem. Lett. 2025, 16, 6627−6636